applied sciences

MDPI

Article

Empirical Quasi-Static and Inverse Kinematics of Cable-Driven Parallel Manipulators Including Presence of Sagging

Phan Gia Luan and Nguyen Truong Thinh *

Department of Mechatronics, HCMC University of Technology and Education, Ho Chi Minh 700000, Vietnam; pgluan95@gmail.com

* Correspondence: thinhnt@hcmute.edu.vn; Tel.: +84-903-675-673

Received: 27 June 2020; Accepted: 24 July 2020; Published: 31 July 2020

Abstract: Cable-driven parallel manipulators (CDPMs) have been of great interest to researchers in recent years because they have many advantages compared to the traditional parallel robot. However, in many studies they lack the cable's elasticity that leads to flexible cables just being considered as extendable rigid links. Furthermore, an external force acts on the extremities of cable and the self-weight is relevant to the length of it. Experimentally, a small change in length produces a huge change in tension act on the entire cable. By this property, the adjusting length of cable is often added to the traditional inverse kinematic solution in order to reduce the tension force exerted on the cable. This means that the load on the actuator is also reduced. Because of the relationship between tension that acts on the cable and its length, the kinematic problem itself does not make sense without concerning the static or dynamic problems. There is often interest in planning forces for actuators and the length of cables based on a given quasi-static trajectory of the moving platform. The mentioned problem is combined with the quasi-static problem with the inverse kinematic problem of CDPM. In this study, we introduce a novel procedure to produce the quasi-static model and inverse kinematic model for CDPM with the presence of sagging by using both an analytic approach and empirical approach. The produced model is time-efficient and is generalized for spatial CDPM. To illustrate the performance of the proposed model, the numerical and experimental approaches are employed to determine particular solutions in the feasible solutions set produced by our model in order to control the two redundant actuators' CDPM tracking on a certain desired trajectory. Its results are clearly described in the experimental section.

Keywords: cable-driven parallel manipulators; overconstrained system; quasi-static; kinematic; sagging cable

1. Introduction

1.1. Motivation

Cable-driven parallel manipulators (CDPMs) are very similar to the traditional parallel robot since they also have a static frame, an end-effector, and many elements that connect the static frame and the end-effector. However, CDPM can easily variate its workspace, which is significantly greater than the other, because the flexible cables are used instead of rigid links. Except for those, they also have other great advantages such as economic structure, transportability, and easy assembling or disassembling [1]. With these outstanding advantages, applications of CDPM can be found in many fields: warehousing in logistics [2], contour crafting system in the construction industry [3], camera system in the stadium, etc. Many CDPMs are enhanced its load capacity also the acceleration by increasing the number of cables. Thus, lots of them have redundant actuators and this kind of structure produces an overconstrained

system [4–6]. Furthermore, the cables that are used to link the end-effector and the robot fixed frame have considerable mass and elasticity, which is mentioned. These kinds of CDPM do not have a unique solution for the statistic or dynamic problem, and the kinematic problem cannot be solved alone. The major problem comes from the deformation of the cables: it increases the length of cables. In practice, these elongations cannot be measured and adjusted, resulting in deviations in the position and orientation of the end-effector. To the best of our knowledge in this field, it is merely impossible to directly extract exact solutions in terms of analysis. Therefore, in the kinematic or dynamic problem, with the given pose of the moving platform, the feasible length of cables and the corresponding tensions are obtained via numerical methods. However, by the complexity of the objective functions, these methods are almost impossible to use in real-time. In order to reduce the complexity of the dynamic problem while preserving the usability of the study, quasi-static problem will be considered in this paper. Similar to the dynamic problem, the quasi-static problem is time-dependent. However, the movement of the moving platform is very slow, or the load is very light, therefore the inertia effect is ignorable. That is very useful in many applications such as contour crafting systems and camera systems, since it simplifies the dynamic problem. In this study, we propose a method that produces the approximated model to solve the quasi-static problem. From that, the length of each cable in which the elongations and the adjusting length are also taken account can be determined in an instant.

1.2. Related Work

Because of its high load capacity and stability, the overconstrained CDPM is an interesting topic for many researchers. As a consequence of the redundant actuators, formulating the model in order to directly obtain the feasible distribution of force in real-time is a challenge. The interval analysis and Levenberg–Marquardt algorithm for real-time forward kinematics are deployed by Pott and Andreas in [7,8]. The same problem in planar CDPM has been studied by Reza Oftadeh et al. in [5] by using extra force sensors. Côté et al. employed quadratic programming method in [9] to handle the tension distribution in the spatial CDPM. Linear programming method is used in [6] to distribute the tension by Lamaury et al. A versatile tension distribution algorithm for two redundant actuators' CDPM was proposed by Gouttefarde, Marc et al. in [10]. That algorithm is based on the properties of a feasible region related to the null space of wrench matrix and unidirectional searching technique. Borgstrom, Per Henrik et al. employed a linear programming approach [11] to determine minimum L^1-norm solution in feasible polyhedron (associated with the null space of wrench matrix). These numerical methods are confirmed as usable in real-time and their results are acceptable. However, not mentioning the elasticity and sagging can cause the degeneration in motion of the large-scale CDPMs. The sagging of the cable can be categorized by the source causing it: elasticity and adjusting length. Elastodynamic problem was analyzed by Han Yuan et al. in [12] by considering the dynamic stiffness of the sagging cable. Nguyen, Dinh Quan et al. are honored to establish a simplified model for cable [13] in static analysis of large-dimension CDPM. The mass and elasticity of cable are taken into account in dual problems: static and kinematic of CDPMs mentioned in [14]. Riehl, Nicolas et al. also used numerical methods to obtain a feasible solution. The combination of interval analysis and the Newton–Raphson scheme, performed to solve the forward kinematics with the presence of sagging cable, is presented in [15]. Although the method proposed by Merlet et al. produces a good solution, it cannot be used in real-time. Another article that uses interval analysis to real-time solve forward kinematics for both elastic and non-elastic cables is shown in [16]. Meanwhile, the methods used in [16] do not deal with saggable cables and ignore the mass of them.

1.3. Contributions

In this study, the quasi-static model and inverse kinematic model of spatial CDPM are constructed by using both an analytic approach and empirical approach. The empirical approach is based on the popular sagging cable model introduced by Irvine [17]. Our Method is valid for the low speed and low

acceleration motion of the moving platform for any kind of spatial CDPM. This is evidenced by results from experiments and simulations detailed in Section 7.

2. Cable-Driven Parallel Manipulators Model

2.1. Sagging Cable Model

In this study, the realistic sagging cable model introduced by Irvine [17] will be used as the standard model in order to derive others. Irvine's sagging cable model is widely used from small-scale to macro applications such as cable-stayed bridge, improving the analysis of CDPM [18], ship anchors analysis, etc. because of the validation for elastic and deformable cable whose mass is considerable. Let consider the cable that has an unstrained length L and one extremity is fixed in the origin of frame $\{A\}$, illustrated in Figure 1. The other extremity **B** was influenced by external force $\mathbf{T} = \begin{bmatrix} T_x & T_z \end{bmatrix}^T$, and we can treat this force as the tension of the cable at free extremity. The reaction force at **A** is denoted as $\mathbf{T'} = \begin{bmatrix} T'_x & T'_z \end{bmatrix}$. Let ρ, E, A be the linear density, Young's modulus, and unstrained cross-section area of the considering cable, respectively. The Cartesian coordinates of a certain point on the cable with respect to $\{A\}$ at the Lagrangian coordinates s is given by Equations (1) and (2).

$$x^A(s) = \frac{T_x^A s}{EA} + \frac{\left|T_x^A\right|}{\rho g}\left[\sinh^{-1}\left(\frac{T_z^A - \rho g(L-s)}{T_x^A}\right) - \sinh^{-1}\left(\frac{T_z^A - \rho g L}{T_x^A}\right)\right] \tag{1}$$

$$z^A(s) = \frac{T_z^A s}{EA} + \frac{\rho g}{EA}\left(\frac{s^2}{2} - Ls\right) + \frac{1}{\rho g}\left[\sqrt{\left(T_x^A\right)^2 + \left(T_z^A - \rho g(L-s)\right)^2} - \sqrt{\left(T_x^A\right)^2 + \left(T_z^A - \rho g L\right)^2}\right] \tag{2}$$

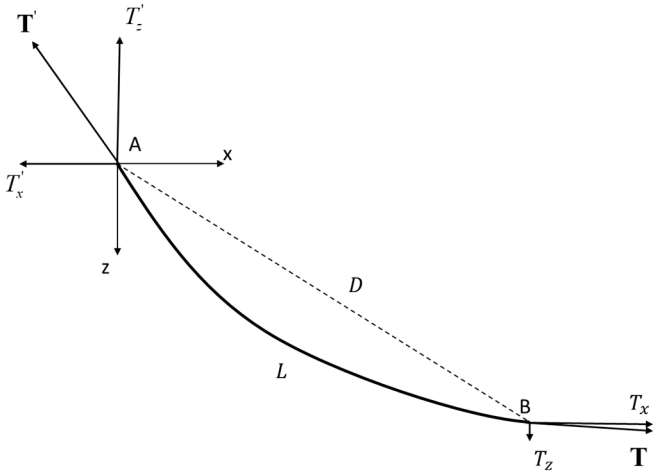

Figure 1. Cable sag model in frame $\{A\}$.

The Cartesian coordinates of extremities of cable respect to $\{A\}$ can be expressed as in (3) and (4).

$$\mathbf{A}^A = \begin{bmatrix} x^A(0) & z^A(0) \end{bmatrix}^T \tag{3}$$

$$\mathbf{B}^A = \begin{bmatrix} x^A(L) & z^A(L) \end{bmatrix}^T \tag{4}$$

2.2. Quasi-Static and Inverse Kinematic Problem of Cable-Driven Parallel Manipulators

The kinematic problem of CDPM that just describes the geometric relationship between a redefined pose of end-effector and the cables' length. However, each cable has its length depend on the tension which acts on it, i.e., the kinematic model alone no longer makes sense. Many works apply the static or dynamic problem to it and solve them simultaneously [3,14–16,19]. Meanwhile, the quasi-static

problem of CDPM concerns finding the proper forces of the moving platform and forces of its constraints given a certain motion of it where the inertial effects are negligible. Once again, with the relationship of tension of each cable and its length, the inverse kinematic problem is solved. Let $\{W\}$ be the reference frame attached to the fixed of CDPM and $\{R\} = (\mathbf{P}(t), \theta(t))$, illustrated in Figure 2, be the moving platform frame attached on its body, where $\mathbf{P} = \begin{bmatrix} x_\mathbf{P} & y_\mathbf{P} & z_\mathbf{P} \end{bmatrix}^T$, $\theta = \begin{bmatrix} \alpha_\mathbf{P} & \beta_\mathbf{P} & \gamma_\mathbf{P} \end{bmatrix}^T$ are the coordinate of center of mass and the vector that represents Euler angle of the moving platform with respect to $\{W\}$. From now on, any vector without a superscript related to any frame is implied to respect to $\{W\}$. We also note that $\mathbf{x} = \begin{bmatrix} \mathbf{P} & \theta \end{bmatrix}^T$ represents the generalized coordinate of the moving platform. If the moving platform is isolated from the system, according to the Newton–Euler's equation, the resultant force $\mathbf{F}$ and torque $\boldsymbol{\tau}$ exert on its center of mass can be obtained via Equation (5)

$$\begin{bmatrix} \mathbf{M} & \mathbf{0} \\ \mathbf{0} & \boldsymbol{\Gamma} \end{bmatrix} \ddot{\mathbf{x}} + \begin{bmatrix} \mathbf{M} \cdot \mathbf{W} & \mathbf{0} \\ \mathbf{0} & \mathbf{W} \cdot \boldsymbol{\Gamma} \end{bmatrix} \dot{\mathbf{x}} + \begin{bmatrix} \mathbf{M} \cdot \mathbf{g} \\ \mathbf{0} \end{bmatrix} = \begin{bmatrix} \mathbf{F} \\ \boldsymbol{\tau} \end{bmatrix} \tag{5}$$

where $\mathbf{M}$ is simplified into the scalar matrix of mass due to the homogeneous density and symmetric geometry of the end-effector, $\boldsymbol{\Gamma}$ is the inertia tensor respect to center of mass of the end-effector expressed in $\{W\}$, $\mathbf{g}$ is the gravitational acceleration vector and $\mathbf{W}$ is the skew symmetric matrix of $\dot{\theta}$. On the other hand, the inertial forces of cables are trivial since the weights of these cables are negligible compared to the end-effector. Thus, if tensions of cables are treated as the external forces of the end-effector, then the resultant force $\mathbf{F}$ and torque $\boldsymbol{\tau}$ also can be expressed as in (6) and (7)

$$F_x = \sum_i -T_{x_i} \quad F_y = \sum_i -T_{y_i} \quad F_z = \sum_i -T_{z_i} - mg \tag{6}$$

$$\tau_x = \sum_i \left(b_{z_i} T_{y_i} - b_{y_i} T_{z_i}\right) \quad \tau_y = \sum_i \left(b_{x_i} T_{z_i} - b_{z_i} T_{x_i}\right) \quad \tau_z = \sum_i \left(b_{y_i} T_{x_i} - b_{x_i} T_{y_i}\right) \tag{7}$$

where $\mathbf{b}_i = \mathbf{B}_i - \mathbf{P}$ is the vector demonstrates the position where the reaction force of tension $\mathbf{T}_i = \begin{bmatrix} T_{x_i} & T_{y_i} & T_{z_i} \end{bmatrix}$ is exerted on the end-effector with respect to $\{R\}$. $\mathbf{b}_i$, given by (8), depends on the rotation matrix $\mathbf{R}_R^W$ that denotes the rotation from $\{R\}$ to $\{W\}$ defined in (9).

$$\mathbf{b}_i = \left(\mathbf{R}_R^W\right)^T \cdot \mathbf{b}_i^R \tag{8}$$

$$\mathbf{R}_R^W = \begin{bmatrix} C_{\alpha_\mathbf{P}} C_{\beta_\mathbf{P}} & C_{\alpha_\mathbf{P}} S_{\beta_\mathbf{P}} S_{\gamma_\mathbf{P}} - S_{\alpha_\mathbf{P}} C_{\gamma_\mathbf{P}} & C_{\alpha_\mathbf{P}} S_{\beta_\mathbf{P}} C_{\gamma_\mathbf{P}} + S_{\alpha_\mathbf{P}} S_{\gamma_\mathbf{P}} \\ S_{\alpha_\mathbf{P}} C_{\beta_\mathbf{P}} & S_{\alpha_\mathbf{P}} S_{\beta_\mathbf{P}} S_{\gamma_\mathbf{P}} + C_{\alpha_\mathbf{P}} C_{\gamma_\mathbf{P}} & S_{\alpha_\mathbf{P}} S_{\beta_\mathbf{P}} C_{\gamma_\mathbf{P}} - C_{\alpha_\mathbf{P}} S_{\gamma_\mathbf{P}} \\ -S_{\beta_\mathbf{P}} & C_{\beta_\mathbf{P}} S_{\gamma_\mathbf{P}} & C_{\beta_\mathbf{P}} C_{\gamma_\mathbf{P}} \end{bmatrix} \tag{9}$$

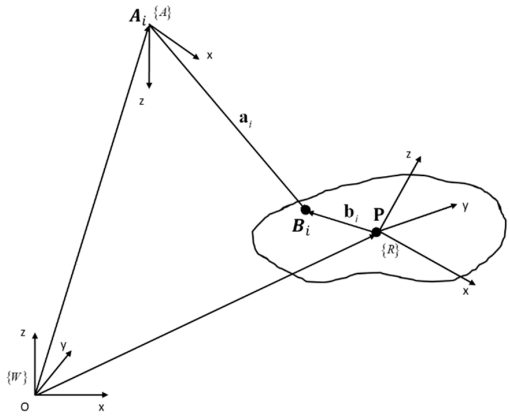

Figure 2. General geometric model of cable-driven parallel manipulators (CDPM).

Naturally, in the ideal statistic condition, or mobile platform moving with speed and acceleration which are not too high, the ith cable profile that is fixed at its extremities $\mathbf{A}_i$ and $\mathbf{B}_i$ completely lies in the plane that contains these points. Similar to the sagging cable model section, let $\{A_i\}$ be the 2D-frame that defines the considered plane and illustrated in Figure 2. We can define $\mathbf{a}_i$ and $\mathbf{T}_i$ respect to $\{A_i\}$ as (10) and (11), respectively

$$\mathbf{a}_i^{A_i} = \mathbf{R}_{A_i}^{W} \cdot \mathbf{a}_i \tag{10}$$

$$\mathbf{T}_i^{A_i} = \mathbf{R}_{A_i}^{W} \cdot \mathbf{T}_i \tag{11}$$

where

$$\mathbf{R}_{A_i}^{W} = \begin{bmatrix} C_{\theta_i} & S_{\theta_i} & 0 \\ 0 & 0 & -1 \end{bmatrix} \tag{12}$$

In the matrix (12), θ_i can be given by (13). Vector $\mathbf{a}_i$ in Equation (10) can be obtained by deploying Equation (14).

$$\theta_i = a\tan 2\left(a_{y_i}, a_{x_i}\right) \tag{13}$$

$$\mathbf{a}_i = \mathbf{P} + \mathbf{b}_i - \mathbf{A}_i \tag{14}$$

According to (11), the equations in (6) and (7) can be expressed as (15) and (16).

$$F_x = \sum_i -T_{x_i}^{A_i}\cos(\theta_i) \quad F_y = \sum_i -T_{x_i}^{A_i}\sin(\theta_i) \quad F_z = \sum_i T_{z_i}^{A_i} - mg \tag{15}$$

$$\tau_x = \sum_i \left(b_{y_i}T_{z_i}^{A_i} + b_{z_i}T_{x_i}^{A_i}\sin(\theta_i)\right) \quad \tau_y = \sum_i \left(-b_{z_i}T_{x_i}^{A_i}\cos(\theta_i) - b_{x_i}T_{z_i}^{A_i}\right) \quad \tau_z = \sum_i \left(-b_{x_i}T_{x_i}^{A_i}\sin(\theta_i) + b_{y_i}T_{x_i}^{A_i}\cos(\theta_i)\right) \tag{16}$$

By changing the frame which the tension relates to, the dimension of distribution forces problem is reduced. From the relationship between the length of cable and a force exerted on it, the solution of both the quasi-static and inverse kinematic problem can be expressed as in (17).

$$\left[\left\{ \begin{array}{ccc} T_{x_i}^{A_i} & T_{z_i}^{A_i} & L_i \end{array} \right\}_{i=1}^{n}\right]^T \tag{17}$$

3. Quasi-Static and Inverse Kinematic Characteristics of Single Cable

Since everything will be discussed in general frame $\{A\}$ in this section, if any vector without a denotation of frame, then this vector respect to $\{A\}$. For the convenience, $\mathbf{T} = \begin{bmatrix} T_x & T_z \end{bmatrix}^T \in \Upsilon$ denotes the tension acts on free extremity $\mathbf{B} = \begin{bmatrix} x_\mathbf{B} & z_\mathbf{B} \end{bmatrix}^T \in \Im$, $\varsigma = \begin{bmatrix} \rho & E & A \end{bmatrix}^T \in \aleph$ denotes the properties of materials that are used in cable, $\mathbf{S} = \begin{bmatrix} T_x & T_z & L \end{bmatrix}^T \in \Delta$ denotes the solution of our study. According to (1), (2) and (4), the sagging cable model of Irvine in [17] can be used to archive the position of the free extremity $\mathbf{B}$ of cable and can be expressed in (18).

$$I : \Delta \times \aleph \to \Im, \begin{bmatrix} \mathbf{S} & \varsigma \end{bmatrix}^T \mapsto \mathbf{B} \tag{18}$$

The main study of this section is try to figure out the feasible tensions and feasible unstrained lengths based on the desired position of the free extremity of cable $\mathbf{B}^d = \begin{bmatrix} x_{\mathbf{B}^d} & z_{\mathbf{B}^d} \end{bmatrix}^T$ with given ς that can be obtained by deploying (19).

$$f : \Im \times \aleph \to \Delta, \begin{bmatrix} \mathbf{B}^d & \varsigma \end{bmatrix}^T \mapsto \mathbf{S} \tag{19}$$

However, the exact (19) cannot be directly derived via (18) by its natural complexity. In previous research, based on given $\mathbf{B}^d$ and the constant material of cable, numerical approaches have been deployed to find out feasible solution $\mathbf{S}$. However, most of these methods cannot be used in real-time because of time-consumption. The approximated models were also introduced in research [13,16,20].

In this work, the approximated model of (19) will be constructed based on (18) by applying both the empirical statistical analysis approach and static analysis approach. Generally, the cost function of our approximated model can be express as Equation (20).

$$\varepsilon = \left|x_{\mathbf{B}^d} - x_{\mathbf{B}}\right| + \left|z_{\mathbf{B}^d} - z_{\mathbf{B}}\right| \tag{20}$$

The optimum model is obtained if $\varepsilon = 0$, $\forall \mathbf{B}^d \in \mathfrak{I}$. However, it is impossible for any approximated model that converges to the actual model, i.e., we always have $\varepsilon > 0$. However, we restrict feasible solutions with the maximum error $\varepsilon < \varepsilon_{\max}$. By using Irvine model with fixed ς and L, a set of feasible tension can be found to satisfy a given desired position $\mathbf{B}^d$. The set of feasible tension of an instance is illustrated in Figure 3.

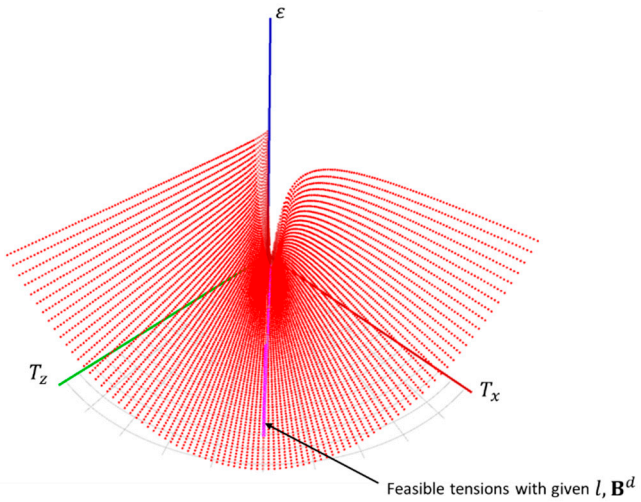

Figure 3. The feasible tensions $\mathbf{T}$ with given L, $\mathbf{B}^d$ and ς with $\varepsilon_{\max} > 0$.

Statement 1. *Let ψ be the feasible tension set with given $\varepsilon_{\max}$, L, $\mathbf{B}^d$ and ς. According to Irvine model, with given L, $\mathbf{T}$ and ς there exists only one $\mathbf{B}$, so (18) is the injective function. Similarly, (19) is also the injective function. Hence, if $\varepsilon_{\max} \to 0$ then $\left|\psi\right| \to 1$, i.e., the set has unique tension $\mathbf{T} \in \psi$.*

Collecting all of ψ with $L \in \mathbb{R}^+$, we can get the feasible solution set Ψ of (19) with given ς and considered $\mathbf{B}^d$ as the input parameter. Figure 4 illustrates a specific case of Ψ with $d = L - D$ and D is the L^2-norm of $\mathbf{B}^d$.

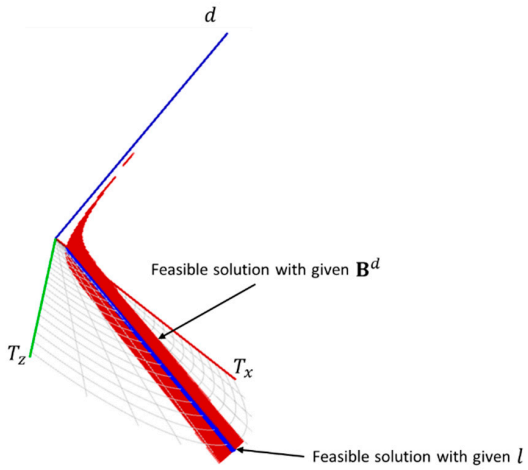

Figure 4. The feasible solutions $\mathbf{S} \in \Psi$ and ψ is the blue segment line with $\varepsilon_{\max} > 0$.

Statement 2. *Let* $\Psi \subset \Pi$ *be the feasible solution set with given* $\mathbf{B}^d$ *and* ς*. If* $\varepsilon_{\max} \to 0$ *then* $\Pi \subset \Delta$ *is the affine plane that contains* Ψ *and its associated vector space that is the orthogonal complement to* Υ *. Thus, the projection of* Ψ *onto* Υ *is the affine line* $\pi \subset \Upsilon$*. Moreover, for each given L value, if* $\varepsilon_{\max} \to 0$ *then there exists only one feasible tension. Therefore,* Ψ *becomes the spatial curve in* Δ*.* π *can be expressed as the relationship between* T_z *and* T_x *in (21)*

$$(\pi) : T_z = a_\pi T_x + b_\pi \tag{21}$$

where a_π *and* b_π *denote the parameters that depend on* $\mathbf{B}^d$ *and* ς*.*

The quasi-static model is established when these parameters are formed in explicit function of $\mathbf{B}^d$. A certain case of π is obtained by using linear regression to fit the projected solution on Υ and it is illustrated in Figure 5.

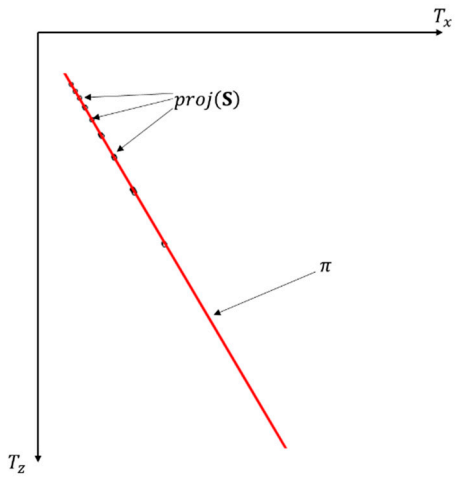

Figure 5. The projection of Ψ onto Υ is the affine line π with given $\mathbf{B}^d$ and ς.

On the other hand, Li, Hui, et al. pointed out the nonlinear relationship between T_z and T_x in [21]. In case of CDPM, the conditions of $\rho gL < w_{\max}$ and $T_x > T_{x_{\min}}$ must be satisfied in order to maintain the stability of the system where $w_{\max}$, $T_{x_{\min}}$ are the maximum self-weight of cable and minimum tension along the X-axis. Moreover, the nonlinear segment of the relationship between T_z and T_x is located at the low part of T_x. Hence, we can ignore the nonlinear part of it and linearize the relationship between T_z and T_x when $\rho gL < w_{\max}$, by employing (21). Moreover, on the simplification of cable model in [13], Nguyen, Dinh Quan et al. proved that if $T \ll EA$, then the elongation of cable caused by elasticity has an ignorable impact on the relationship between T_z and T_x. This is also proved in [20]. In fact, the above assumption is always satisfied since cables used in CDPM often have very high stiffness to withstand the load of the mobile platform. Therefore, a_π and b_π now just depend on $\mathbf{B}^d$ and ρ. In Section 4, we will figure out the quasi-static model of a single cable by combining an analytical approach and empirical approach.

4. Empirical Quasi-Static Model of Single cable

4.1. Analyze the Natural Limit of Tension Act on Free Extremity of Cable

Let m, α be the magnitude and direction of $\mathbf{T}$ respect to the X-axis, respectively. Let β be the angle between $\mathbf{AB}$ and the X-axis. The direction of $\mathbf{T}$ can be expressed as (22).

$$\alpha = \tan^{-1}\left(\frac{T_z}{T_x}\right) \tag{22}$$

Since the relationship between T_z and T_x can be considered as (21), Equation (22) can be rewritten as (23).

$$\alpha = \tan^{-1}\left(a_\pi + \frac{b_\pi}{T_x}\right) \tag{23}$$

In reality, we know that $\mathbf{T} \neq -\mathbf{T}'$ where $\mathbf{T}'$ is the reaction force at **A** illustrated in Figure 1 due to the self-weight of the cable. Since **T** and $\mathbf{T}'$ tangent to the cable at extremities **A** and **B**, respectively, there is always the sagging in the cable. This explains the phenomenon of not being able to straightly stress the cable. However, if $|T_z| \gg \rho g L$, then we can ignore the mass of cable and $\mathbf{T} + \mathbf{T}' \to 0$ that leads to $\alpha \to \beta$. This can be expressed as (24).

$$\lim_{|T_z| \to \infty} \alpha = \beta \tag{24}$$

According to (21) and (23), if $|T_z| \to \infty$ and $a_\pi \neq 0$, then $|T_x| \to \infty$ that leads to $\alpha \to \tan^{-1}(a_\pi)$. This process can be given by (25).

$$\lim_{|T_z| \to \infty} \alpha = \lim_{|T_x| \to \infty} \left(\tan^{-1}\left(a_\pi + \frac{b_\pi}{T_x}\right)\right) = \tan^{-1}(a_\pi) \tag{25}$$

From (24) and (25), we can conclude that if (21) is considered as the relationship between T_x and T_z, then the slope a_π just depends on β and be expressed as (26).

$$a_\pi = \tan(\beta) \tag{26}$$

4.2. Empirical Relationship between b_π and [$\mathbf{B}^d$ ρ]

4.2.1. Relationship between b_π and D

In order to comfortably obtain the complete relationship between b_π and $\begin{bmatrix} D & \beta & \rho \end{bmatrix}$, the relationship between b_π and one of the mentioned parameters are considered first and that results in new parameters. These parameters now just depend on the rest and so we recursively repeat the procedure until the last parameter. In our case, the order of execution will be D, ρ and β. By variating D, fixing β and ρ, and using linear regression to establish (21), the relationship between b_π and D can be guessed by forming the scatter plot in Figure 6.

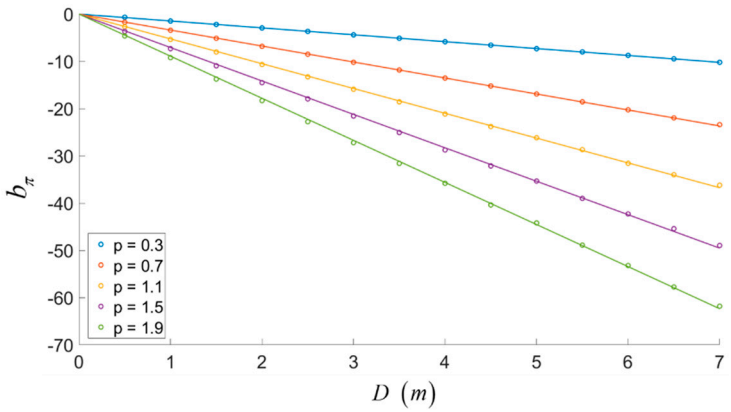

Figure 6. Relationship between b_π and D with different ρ.

According to the results illustrated in Figure 6, the relationship between b_π and D can be expressed as in Equation (27). The parameter of this equation changes if ρ changes.

$$b_\pi = h_b(\rho) \cdot D \tag{27}$$

4.2.2. Relationship between h_b and ρ

In Figure 7, the values of h_b are plotted with given discrete $\rho \in (0, 2)$ and fixed β. It is easy to state that h_b and ρ are linearly decreasing in the considered open set. Furthermore, when β is variated, the relationship between h_b and ρ does not change, i.e., h_b does not depend on β. Thus, the relationship between h_b and ρ can be expressed as $h_b = k_h \cdot \rho$, where k_h is a constant.

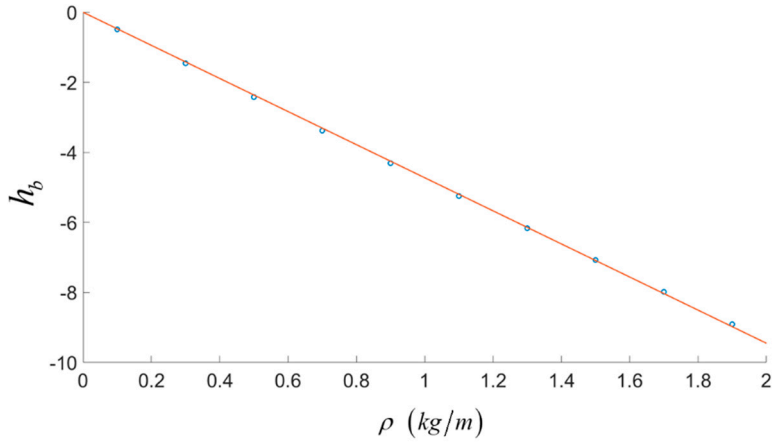

Figure 7. The relationship between β and h_b with given ς.

Based on our taken data and proposed procedure, we have $k_h \approx -4.845$. This parameter can be approximately equal to negative half of gravitational acceleration. Following this assumption, the relationship between h_b and ρ can be expressed as (28).

$$h_b = -\frac{\rho g}{2} \tag{28}$$

The obtained parameter h_b based on our procedure coincides with the simplified cable model introduced in [20].

4.3. Relationship between T_z and T_x

In Statement 2, we state that $T_z = a_\pi T_x + b_\pi$ with a_π and b_π depend on $\mathbf{B}^d$ and ρ. According to Equations (26) and (27), the relationship between T_z and T_x can be expressed as Equation (29).

$$T_z = \tan(\beta) T_x + h_b D \tag{29}$$

Substituting the parameter (28) to (29), the affine line π can be expressed as the set (30).

$$\pi = \left\{ (T_x, T_z) : T_z = \tan(\beta) T_x - \frac{\rho g D}{2} \right\} \tag{30}$$

The second statement pointed out that the solution of the quasi-static problem of single cable is not unique and the particular solution just can be resolved when the cable unstrained length L is determined. In Section 5, we will try to establish the relationship between cable tension act on the extremity $\mathbf{B}$ and the unstrained length of cable by using both analytical approach and empirical approach.

5. Relationship between Cable Unstrained Length and Cable Tension

5.1. Simplify the Problem

In order to formulate the relationship between L and $\mathbf{T}$, Ψ that is the set of all feasible solutions $\mathbf{S}$ of (19) with given desired position $\mathbf{B}^d$ and ς, must be established. However, the construction of Ψ

directly is not simple. Meanwhile, in Statement 2, we assumed that $\Psi \subset \Pi$, as long as $\rho g L < w_{\max}$ and $T_x > T_{x_{\min}}$. By successfully constructing the projection of Π onto the Υ, π, the relationship between T_x and T_z was obtained. Hence, the relationship between L and $\mathbf{T}$ can be formed by constructing the relationship between L and any component of tension such as T_x, T_z, T, α instead of directly constructing Ψ.

Since the relationship between T_z and T_x is described as (21), if $b_\pi \neq 0$ then the minimum magnitude of tension $T_{\min}$ that satisfies a certain point $\mathbf{B}^d$ with $0 < \beta < 90^\circ$ and $D > 0$, is always greater than 0, i.e., the function that expresses the relationship between L and T has its vertical asymptote that can be estimated as (31)

$$T_{\min} = \frac{|b_\pi|}{\sqrt{{a_\pi}^2 + {b_\pi}^2}} \tag{31}$$

where a_π and b_π are the parameters that define π. On the other hand, when T_x or T_z is considered instead of T, the vertical asymptotes of the function that expresses the relationship between T_x or T_z, and d are $T_x = 0$ or $T_z = b_\pi$ respectively. Hence, to ease the calculation and effortlessly identify the model, T_x is chosen. Moreover, we have $L = D + d$ and D is determined so the relationship between L and T_x can be replaced by d and T_x. Let Ψ be the new solution set that can be expressed as (32).

$$\Psi = \{(T_x, d) : d = d(T_x)\} \tag{32}$$

Theoretically, if the cable is unstretchable then the adjusting length d cannot be lesser than 0 and vice versa. Ψ of unstretchable cable and stretch cable with given certain $\mathbf{B}^d$ and ς are illustrated in the Figure 8.

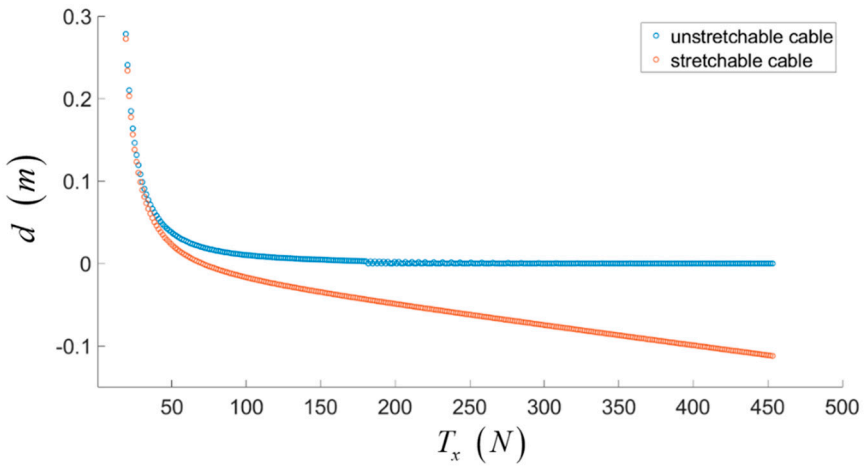

Figure 8. The relationship between d and T_x of both of unstretchable and stretchable cable in the instance.

The negative part of d of the stretchable cable illustrated in Figure 8 is caused by the elasticity of the cable and it has the boundary that obeys Hooke's law. In general, modelling Ψ in the case of unstretchable cable is easier, since it has $d = 0$ as its horizontal asymptote. Meanwhile, Ψ in the case of stretchable cable has an inclined asymptote.

To avoid misunderstanding, from now on, L denotes the unstrained length of stretchable cable. Let s and $\Delta l(s)$ be the Lagrangian coordinates of an unstrained stretchable cable and elongation of the cable under external force at s, respectively. $\Delta l(s)$ can be formulated as Equation (33)

$$\Delta l(s) = \sqrt{\Delta l_x(s) + \Delta l_z(s)} \tag{33}$$

where Δl_x, Δl_z are the strained length of cable at s along the X and Z axis, respectively. They can be formed by Equations (34) and (35), derived from Hooke's law.

$$\Delta l_x(s) = \frac{T_x s}{EA} \tag{34}$$

$$\Delta l_z(s) = \frac{T_z s}{EA} - \frac{\rho g(L-s)s}{EA} \tag{35}$$

Substituting (34), (35) to (33), the relationship between the elongation of overall cable and tension can be formulated by (36)

$$\Delta l = \frac{TL}{EA} \tag{36}$$

where $\Delta l = \Delta l(L)$. In terms of T_x, (36) can be written as (37).

$$\Delta l = \frac{\sqrt{{T_x}^2 + (a_\pi T_x + b_\pi)^2} \cdot L}{EA} \tag{37}$$

Considering a stretchable cable, let $L^e = D + d^e + \Delta l$ be the strained length of it where d^e is the adjusted length of stretchable cable and satisfies a certain point, $\mathbf{B}^d$, with given tension $\mathbf{T}^e$. According to statement 1, we can state that there exists the unique tension, $\mathbf{T}$, that satisfies the same desired position, $\mathbf{B}^d$, when unstretchable cables are concerned, with a given cable length that equals the strained length of stretchable cable, i.e., $L^e = D + d$. Following that, we can obtain Equation (38).

$$d = d^e + \Delta l \tag{38}$$

By applying Equation (38) to Ψ associated with stretchable cable, the approximated relationship between d and T_x can be archived. In Figure 9, the blue dot illustrated Ψ taken from an Irvine model with given certain $\mathbf{B}^d$ when the elongation part is removed. The red dot illustrated Ψ associated with stretchable cable when the elongation part is removed by (38).

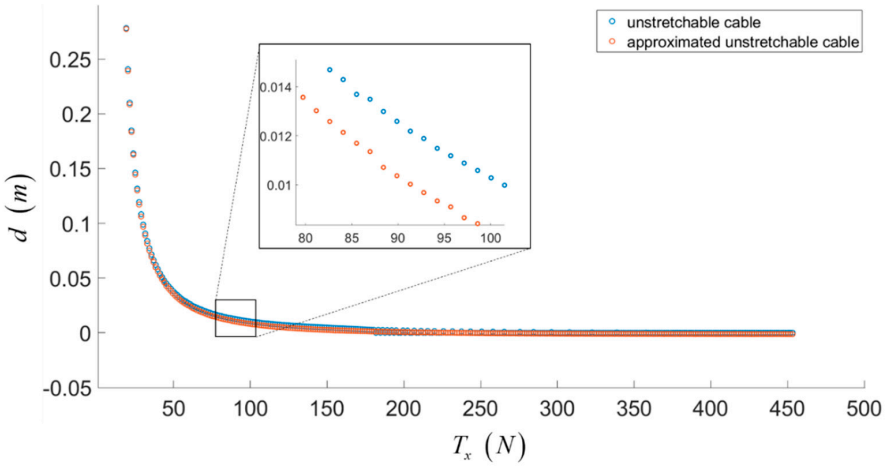

Figure 9. The relationship between d and m that concerns to the unstretchable cable and the approximated one.

According to the result that is illustrated in Figure 9, the feasible solution set Ψ can be expressed as (39) instead of (32)

$$\Psi = \left\{(T_x, d) : d\left(T_x, \mathbf{B}^d\right) = d^e\left(T_x, \mathbf{B}^d\right) - \Delta l\left(T_x, \mathbf{B}^d\right)\right\} \tag{39}$$

where (T_x, d) satisfies a certain point $\mathbf{B}^d$ when considering the unstretchable cable.

5.2. Relationship between d and T_x

5.2.1. Select Model

Experimentally, the rational model (40) was chosen in order to estimate Ψ. The rational model (40) that has a constant numerator and 2nd order demonstrator, has an adjustable vertical asymptote based on a_d, and horizontal asymptote $d = 0$. Furthermore, this model is the fittest and simplest that we tried our best to figure out.

$$d = \frac{a_d}{{T_x}^2 + b_d T_x + c_d} \tag{40}$$

Since the vertical asymptote of Ψ is $T_x = 0$, by the properties of (40), we have $b_d = 0$ and $c_d = 0$. Hence, the model is simplified to (41)

$$d = \frac{a_d}{{T_x}^2} \tag{41}$$

where a_d depends on the desired position $\mathbf{B}^d$ and ρ that can be expressed as (42). The only constraint of a_d is $a_d \geq 0$ since $d \geq 0$.

$$a_d = a_d(D, \beta, \rho) \tag{42}$$

Similar to constructing π, Equation (42) will be constructed based on the model (41) when one variable is variated and the others are fixed. Hence, the recently constructed model may have parameters that depend on variables that have not been investigated. In our case, the order of investigating parameters will be D, β and ρ.

5.2.2. Relationship between a_d and D

By fixing $\mathbf{B}^d$ and ρ, the adjusted length d that corresponds to a certain T_x is obtained by optimizing (20). The relationship of d and T_x is modeled by using nonlinear regression with respect to (41). The result is illustrated in Figure 10 with diversity of D.

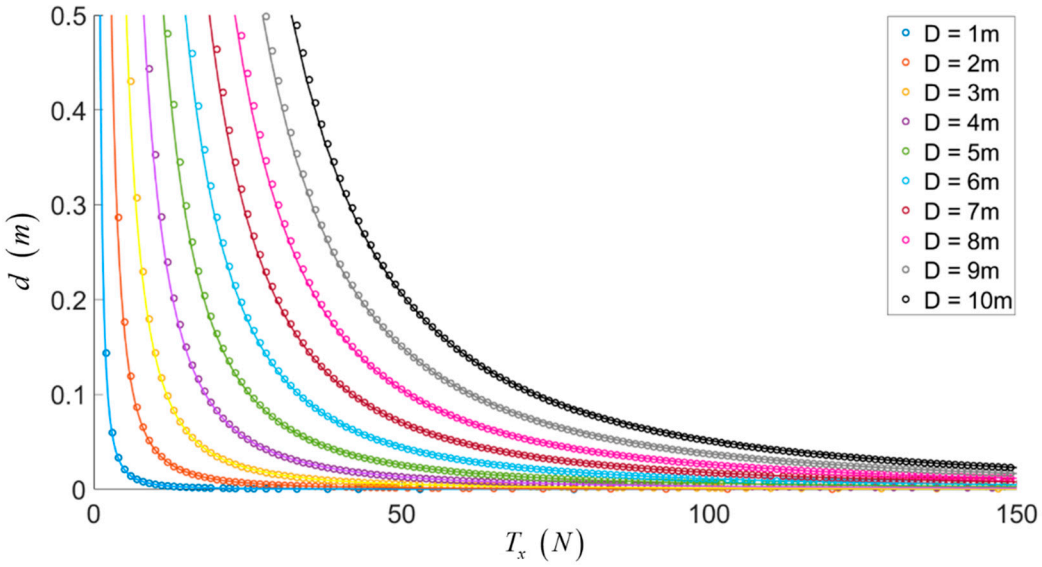

Figure 10. The relationship between T_x and d with different D and fixed $\beta = 0.754$ rad.

In reality, if $D \to 0$, then $\mathbf{B}^d \to \mathbf{A}$, which leads to $T_x \to 0$ and $d \in \mathbb{R}^+$. According to (41), the consequence of $D \to 0$ is $a_d \to 0$. That is also proven in Figure 11. Hence, the model estimated that the relationship between a_d and d cannot have terms that are independent of D. Furthermore, if $D \to \infty$ and d is a finite number, then $L \to D$, which leads to $T_x \to \infty$. According to (41), if $D \to \infty$ then $a_d \to \infty$. By its monotonic property, the function that expresses the relationship between a_d and D cannot have extrema.

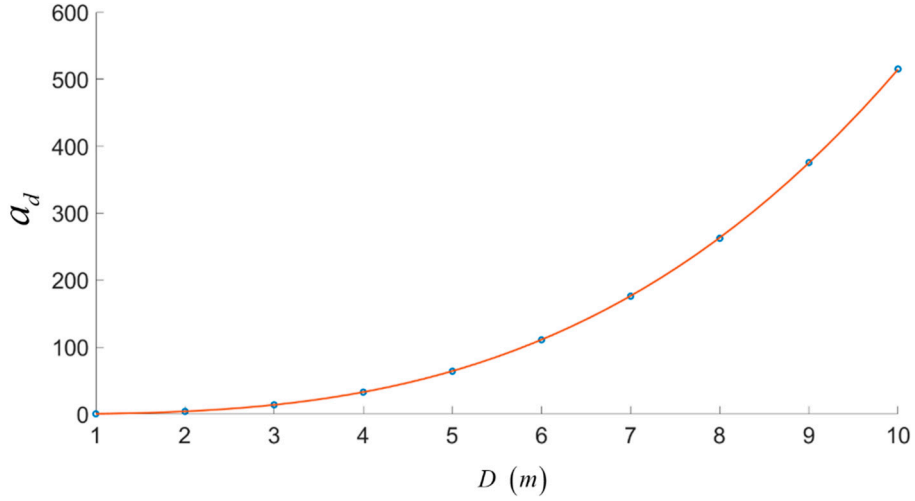

Figure 11. The relationship between D and p.

According to these analyzes, either the power model or exponential model can be used to estimate the relationship between D and a_d. However, the 3rd order power model (43) is the fittest model to the collected data. In the next step, β will be variated with fixed ρ.

$$a_d = q_a(\beta) \cdot D^3 \tag{43}$$

The relationship (43) is always valid with constraint $a_d \geq 0$ since $D \geq 0$.

5.2.3. Relationship between β and q_a

According to (43), each certain β gives us one value of q_a and each value of q_a gives us one curve expressed as the relationship between a_d and D. Those curves are illustrated in Figure 12. By variating β, we can plot the relationship between q_a and β, which is illustrated in Figure 13.

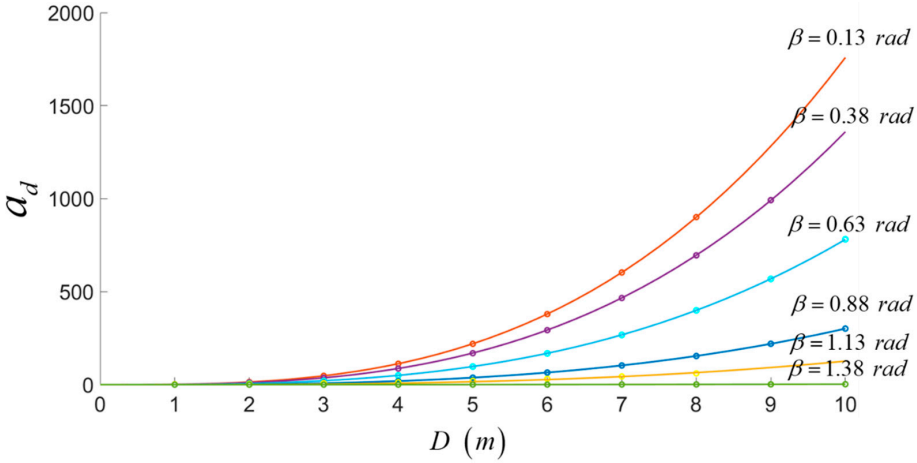

Figure 12. The relationship between D and a_d with different β.

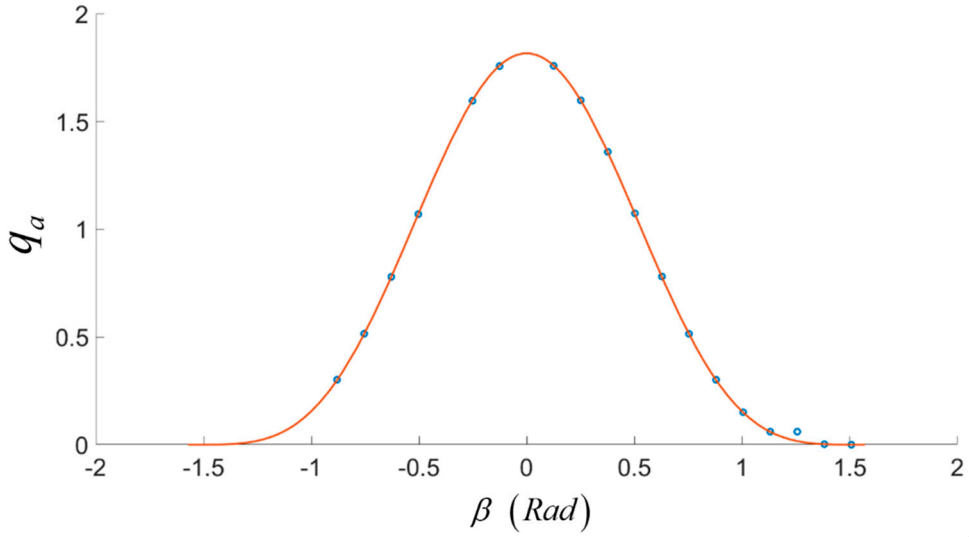

Figure 13. The relationship between β and q_a.

According to the result in Figure 13, the periodic function is valid with the relationship between β and q_a. To satisfy the constraint $a_d \geq 0$, the equation that expresses this relationship should have absolute value. Experimentally, the model (44) was chosen in order to estimate the relationship between β and q_a. Once again, p_q is the parameter that depends on ρ.

$$q_a = p_q(\rho) \cdot \cos^4(\beta) \tag{44}$$

5.2.4. Relationship between p_q and ρ

Similar to the procedure in relationship between h_b and ρ, the relationship between p_q and ρ will be investigated discretely in $\rho \in (0, 2)$. The Figures 14 and 15 show the relationship (44) with different ρ, and the relationship between p_q and ρ, respectively.

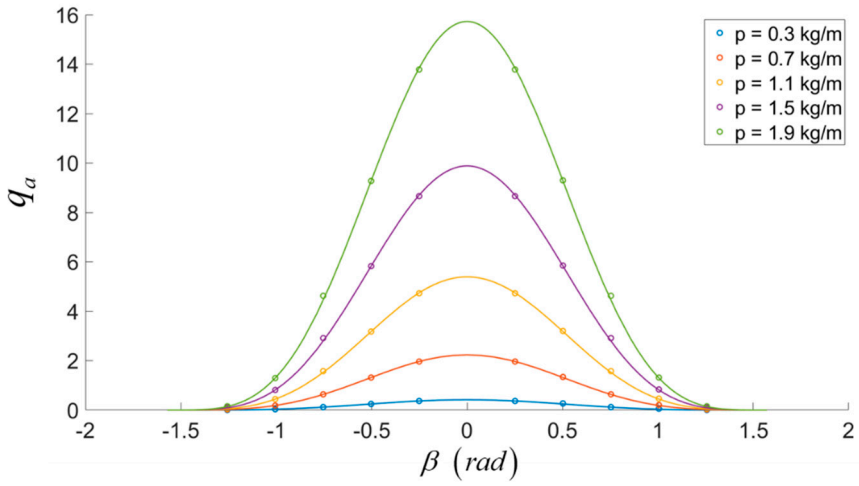

Figure 14. The relationship between β and q_a with different ρ.

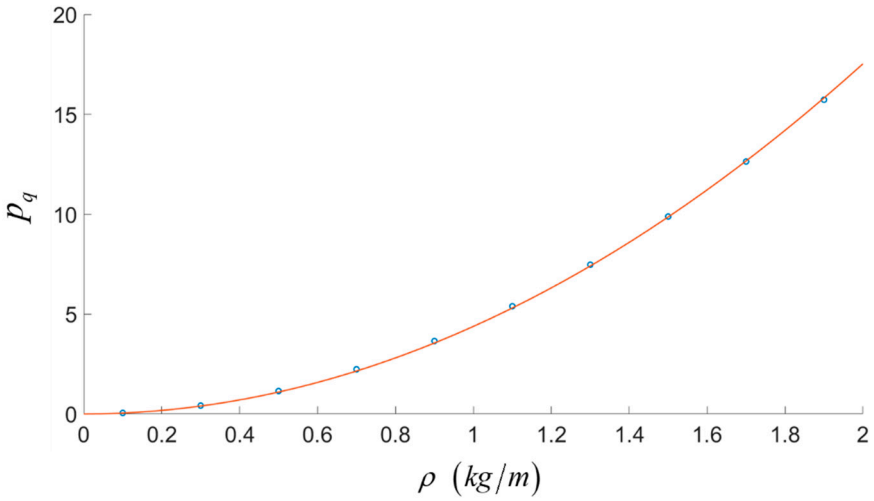

Figure 15. The relationship between p_q and ρ.

According to these results, the model (45) can be used to estimate this relationship, since it is the simplest and fittest model for our gathered data. Furthermore, it is also valid to the constraint $a_d \geq 0$.

$$p_q = k_p \rho^2 \tag{45}$$

However, we cannot exactly formulate k_p due to the errors in the established model. Thus, k_p will be treated as the constant. Based on the non-linear regression method, we have $k_p \approx 4.385$.

5.2.5. Relationship between L and T_x

Substituting (37) and (41) to (38), the adjusted length in stretchable cable d^e can be expressed as (46).

$$d^e = \frac{a_d}{{T_x}^2} - \frac{\sqrt{{T_x}^2 - (a_\pi T_x + b_\pi)^2} \cdot L}{EA} \tag{46}$$

Based on the relationship between a_d and D, β, Equation (46) turns to (47).

$$d^e = \frac{k_p \rho^2 \cos^4(\beta) D^3}{{T_x}^2} - \frac{\sqrt{{T_x}^2 - (a_\pi T_x + b_\pi)^2} \cdot L}{EA} \tag{47}$$

Since $L = D + d^e$, the explicit function L in terms of T_x is given by (48).

$$L = \frac{k_p EA \rho^2 \cos^4(\beta) D^3 - {T_x}^2 EAD}{{T_x}^2 \left(EA + \sqrt{{T_x}^2 - (a_\pi T_x + b_\pi)^2} \right)} \tag{48}$$

The equation of (48) is the explicit function of the unstrained length L of stretchable cable and the tension along the X-axis, T_x. We also need to pay attention to parameters D and β, presented in (48). These parameters represent the position of extremity $\mathbf{B}^d$. Hence, (48) can be treated as the inverse kinematic model of a single cable.

6. From Quasi-Statics to Inverse Kinematics of Cable-Driven Parallel Manipulators

The equations in (15), (16) describe the total force and total torque that act on the end-effector respect to $\{W\}$. By substituting Equations (21) to (15), (16), these equations are fully expressed by the

geometric parameters and properties of material of the cable with variables in terms of T_x^A. It can be given as the system of Equation (49)

$$\mathbf{H} \cdot \mathbf{t}_x + \mathbf{b} = \begin{bmatrix} \mathbf{F} \\ \tau \end{bmatrix} \tag{49}$$

where $\mathbf{H}$ is given as the matrix (50), $\mathbf{t}_x = \begin{bmatrix} T_{x_1}^A & T_{x_2}^A & \dots & T_{x_n}^A \end{bmatrix}^T$ is the vector of tensions along X-axis with respect to $\{A\}$ and $\mathbf{b}$, expressed as (51), is the vector of free coefficients related to T_x^A.

$$\mathbf{H} = \begin{bmatrix} -\cos(\theta_1) & -\cos(\theta_2) & \dots & \dots & -\cos(\theta_n) \\ -\sin(\theta_1) & -\sin(\theta_2) & \dots & \dots & -\sin(\theta_n) \\ a_{\pi_1} & a_{\pi_2} & \dots & \dots & a_{\pi_n} \\ b_{y_1}a_{\pi_1} + b_{z_1}\sin(\theta_1) & b_{y_2}a_{\pi_2} + b_{z_2}\sin(\theta_2) & \dots & \dots & b_{y_n}a_{\pi_n} + b_{z_n}\sin(\theta_n) \\ -b_{z_1}\cos(\theta_1) - b_{x_1}a_{\pi_1} & -b_{z_2}\cos(\theta_2) - b_{x_2}a_{\pi_2} & \dots & \dots & -b_{z_n}\cos(\theta_n) - b_{x_n}a_{\pi_n} \\ -b_{x_1}\sin(\theta_1) + b_{y_1}\cos(\theta_1) & -b_{x_2}\sin(\theta_2) + b_{y_2}\cos(\theta_2) & \dots & \dots & -b_{x_n}\sin(\theta_n) + b_{y_n}\cos(\theta_n) \end{bmatrix} \tag{50}$$

$$\mathbf{b} = \begin{bmatrix} 0 & 0 & \sum_{i=1}^{n} b_{\pi_i} - mg & \sum_{i=1}^{n} b_{\pi_i} b_{y_i} & -\sum_{i=1}^{n} b_{\pi_i} b_{x_i} & 0 \end{bmatrix}^T \tag{51}$$

Equation (5) gives us the wrench of end-effector respect to the redefined motion of the end-effector. Meanwhile, the wrench of end-effector, which is calculated based on a set of tensions, is given by Equation (49). Since we only investigated the active segment of cable, the wrench involved in friction on the pulley can be ignored. Therefore, Equation (49) can be substituted to (5) and expressed as the quasi-static model of the CDPM (52).

$$\left(\mathbf{H}^T\mathbf{H}\right)^{-1}\mathbf{H}^T\left\{\begin{bmatrix} \mathbf{M} & 0 \\ 0 & \mathbf{\Gamma} \end{bmatrix}\ddot{\mathbf{x}} + \begin{bmatrix} \mathbf{M}\cdot\mathbf{W} & 0 \\ 0 & \mathbf{W}\cdot\mathbf{\Gamma} \end{bmatrix}\dot{\mathbf{x}} + \begin{bmatrix} \mathbf{M}\cdot\mathbf{g} \\ 0 \end{bmatrix} - \mathbf{b}\right\} = \mathbf{t}_x \tag{52}$$

In CDPM, the inverse kinematic problem relates to figuring out the length of each cable according to the given motion of the moving platform. The traditional inverse kinematic model is only suitable for robots that have rigid links. Meanwhile, the CDPM links between end-effector and fixed frame are flexible and elastic, i.e., the length of its link is respect to the load distribution. This is evidence of having independently done the quasi-static problem before the solution of the inverse kinematic problem was determined by Equation (48). With the given motion of end-effector $\mathbf{x}(t)$, the solution of this hybrid problem can be determined by applying the overall procedure illustrated in Figure 16.

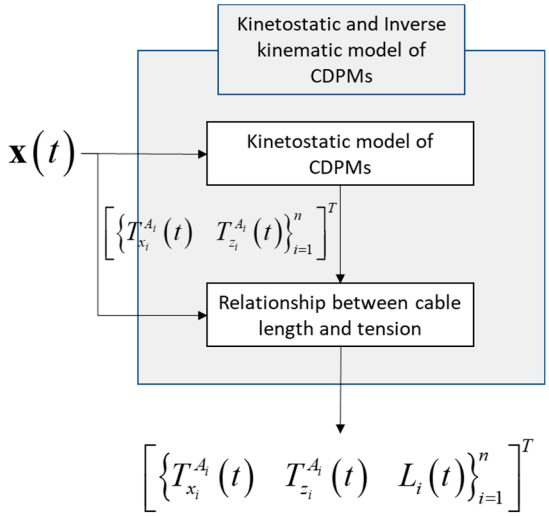

Figure 16. The proposed method used to obtain (17) based on given motion of end-effector.

The trajectory is fed to these models: the quasi-static models of CDPM are considered first. The final result is obtained by passing the results of the quasi-static model of CDPM block together with the trajectory of end-effector to the relationship between cable length and tension block. That block can be considered as a pseudo-inverse-kinematic model of CDPM. In next section, we will employ this model into a series of experiment in order to verify its capacities.

7. Experiments and Results

In this section, the series of experiment and its results will be divided into two parts: simulation and experiment. All experiments are applied to over-constrained system with two redundant actuators because of their high popularity and application. Other parameters of the robot are mentioned in Table 1. In order to confirm the availability of the proposed model for any spatial CDPM, we considered a simulation test with two CDPM. They have the same number of cables and related parameters as summarized in Table 2, but they have different a configuration, illustrated in Figure 17. From that, we can compare the performance of the proposed model in these configurations.

Table 1. Parameters of CDPMs used in experiment and simulation.

Parameters	Experiment	Simulation
Fixed frame size	3 m × 6 m × 3 m	15 m × 11 m × 6 m
End-effector size	0.3 m × 0.3 m × 0.5 m	0.3 m × 0.3 m × 0.5 m
End-effector load	50 kg	50 kg
ρ	0.09 kg/m	0.067 kg/m
E	3.5 GPa	2 GPa
A	4 mm^2	2 mm^2

Table 2. Performance of model in our CDPM based on set of static poses.

Desired Positions (m)	Actual Position (m)	Positioning Error (mm)
$\mathbf{P_1}$(0.22, −0.45, 1.43)	(0.2220, −0.4510, 1.4470)	17.1464
$\mathbf{P_2}$(−0.13, 1.42, 0.68)	(−0.1290, 1.4380, 0.7210)	44.7884
$\mathbf{P_3}$(−0.29, −0.25, 1.52)	(−0.2920, −0.2510, 1.5340)	14.1774
$\mathbf{P_4}$(0.30, 1.26, 2.31)	(0.3000, 1.2610, 2.3150)	5.0990
$\mathbf{P_5}$(−0.47, 0.80, 2.17)	(−0.4710, 0.8000, 2.1760)	6.0828
$\mathbf{P_6}$(0.48, −0.85, 0.72)	(0.4860, −0.8550, 0.7460)	27.1477
$\mathbf{P_7}$(−1.08, −0.75, 2.54)	(−1.0810, −0.7510, 2.5410)	1.7321
$\mathbf{P_8}$(0.26, 1.06, 0.44)	(0.2640, 1.0760, 0.4790)	42.3438
$\mathbf{P_9}$(0.45, −1.73, 1.71)	(0.4500, −1.7340, 1.7270)	17.4642
$\mathbf{P_{10}}$(0.67, 0.52, 2.02)	(0.6710, 0.5200, 2.0280)	8.0623

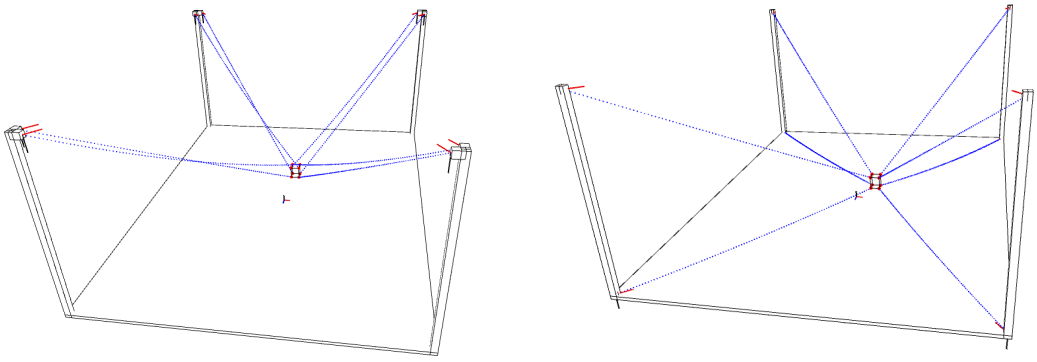

(**a**) (**b**)

Figure 17. (**a**) The first configuration; (**b**) the second configuration used in simulation test.

7.1. Simulation

In reality, there are many means of 8-cable CDPM wiring, so we tried to offer the two most common configurations. Both configurations mentioned in this section have symmetric geometry. Figure 17a depicts the configuration where all eight wires are attached to top of the workspace and the other depicts the configuration where four wires are attached to top of the workspace and the remaining are attached to the bottom of the workspace. These configurations can be found in many prototypes. The first one is famous thanks to the introduction of CoGiRo, and also considers the optimal geometry of two redundant actuators suspended CDPM [22]. IPAnema1, presented by Pott, Andreas et al. in [23], is the well-known prototype of the second configuration illustrated in Figure 17b. In this experiment, the moving platform of simulated CDPM is expected to track on the desired trajectory illustrated in Figure 18 with the given constraint $\begin{bmatrix} z_{\mathbf{P}} & \alpha_{\mathbf{P}} & \beta_{\mathbf{P}} & \gamma_{\mathbf{P}} \end{bmatrix} = \begin{bmatrix} 1.5 & 0 & 0 & 0 \end{bmatrix}$. The 5th order polynomial control equations are applied in order to generate this trajectory. Time-based velocities of the end-effector along the X-axis and Y-axis are illustrated in Figure 19.

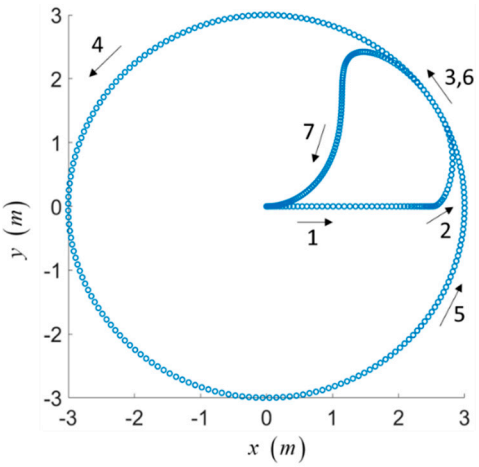

Figure 18. The trajectory of moving platform for simulation test.

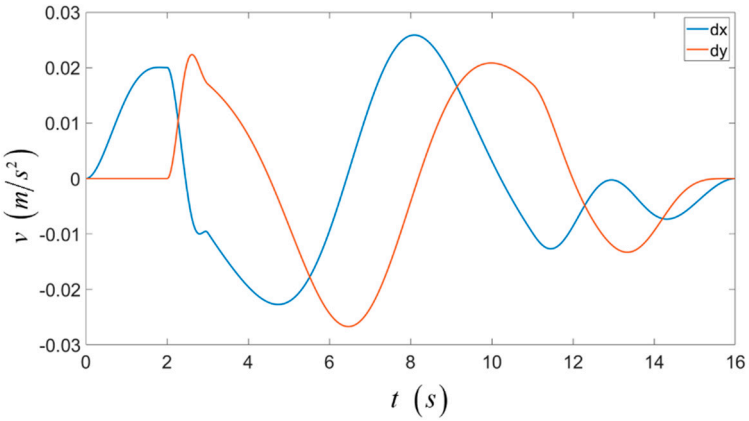

Figure 19. The velocity of moving platform in desired trajectory.

Because the mentioned CDPMs in this section are overconstrained systems, there is a presence of the non-unique pseudo inverse of (50). To illustrate the performance of our model during tracking on the desired trajectory, a simple numerical approach is employed to solve that issue. The goal of this procedure is to find out a smooth series of minimum tensions which also satisfies the desired trajectory

and constraints of our proposed model. Firstly, the particular solution $\mathbf{t}_{x_0} = \begin{bmatrix} T^A_{x_{1_0}} & T^A_{x_{2_0}} & \cdots & T^A_{x_{8_0}} \end{bmatrix}^T$ of (49) is a minimum L^2 norm solution. The general solution of (49) can be expressed as (53)

$$\mathbf{t}_x = \mathbf{t}_{x_0} + \mathbf{N}\boldsymbol{\lambda} \tag{53}$$

where $\mathbf{N}$ is the 8×2-matrix that represents the orthonormal basis for the null space of $\mathbf{H}$ and the particular solution $\mathbf{t}_x$ of (49) depends on the value of $\boldsymbol{\lambda} = \begin{bmatrix} \lambda_1 & \lambda_2 \end{bmatrix}^T$. The constraint of (53) is introduced, and can be written as (54)

$$\mathbf{t}_x > \mathbf{t}_{x_{\min}}, T_{x_{i\min}} = \frac{-\mathrm{b}_{\pi_i}}{\mathrm{a}_{\pi_i}} + T_{x_i adj}, T_{x_i adj} > 0 \tag{54}$$

where $\mathbf{t}_{x_{\min}} = \begin{bmatrix} T^A_{x_{1_{\min}}} & T^A_{x_{2_{\min}}} & \cdots & T^A_{x_{8_{\min}}} \end{bmatrix}$. In fact, the addition of $T^A_{x_{i_{adj}}}$ to maintain the accuracy of our proposed model as we discussed in Section 3. Applying the constraint (54) to Equation (53), the feasible solution set Θ_λ is obtained and it is surrounded by a planar polygon. The polygonal boundary of Θ_λ is defined by the vertex set $\Omega_\lambda = \{\boldsymbol{\lambda}_i\}_{i=1}^h$.However, the obtained feasible solution set Θ_λ is presented in the domain of $\mathbf{N}$. Since we cannot directly determine suitable $\mathbf{t}_x$ in that space, Θ_λ is transformed to new set $\Theta_\mathbf{t}$ presented in the null space of $\mathbf{H}$ by executing the linear affine transformation (53) to set Ω_λ, resulting in a new vertex set $\Omega_\mathbf{t} = \left\{\mathbf{t}_{x_i}\right\}_{i=1}^h$ that defines the $\mathbb{R}^8$-polygon. The kth particular solution ${}^k\mathbf{t}_x$ is selected based on ${}^{k-1}\mathbf{t}_x$. To produce the smooth series of the minimum L^2-norm solution, we will select ${}^k\mathbf{t}_x$ by optimizing the objective function (55).

$$\min_{{}^k\mathbf{t}_x \in {}^k\Theta_t} \|{}^k\mathbf{t}_x - {}^{k-1}\mathbf{t}_x\| \tag{55}$$

The results of this experiment, obtained by employing our proposed model and the numerical method mentioned above, are illustrated in Figures 20 and 21.

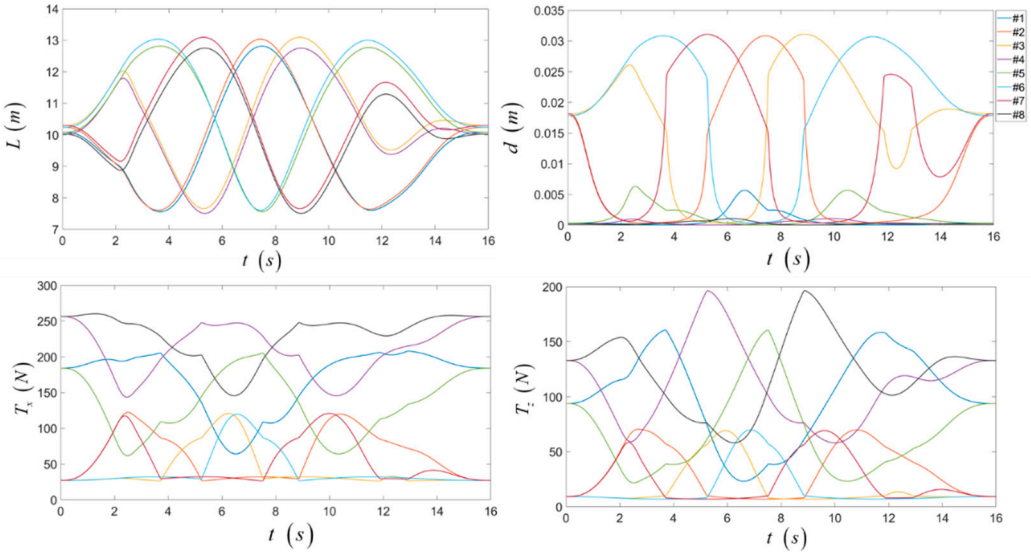

Figure 20. Unstrained length L, adjusting length d, tension along X-axis T_x and tension along Z-axis T_z respect to $\{A\}$ of CDPM that has the first configuration during the simulation test.

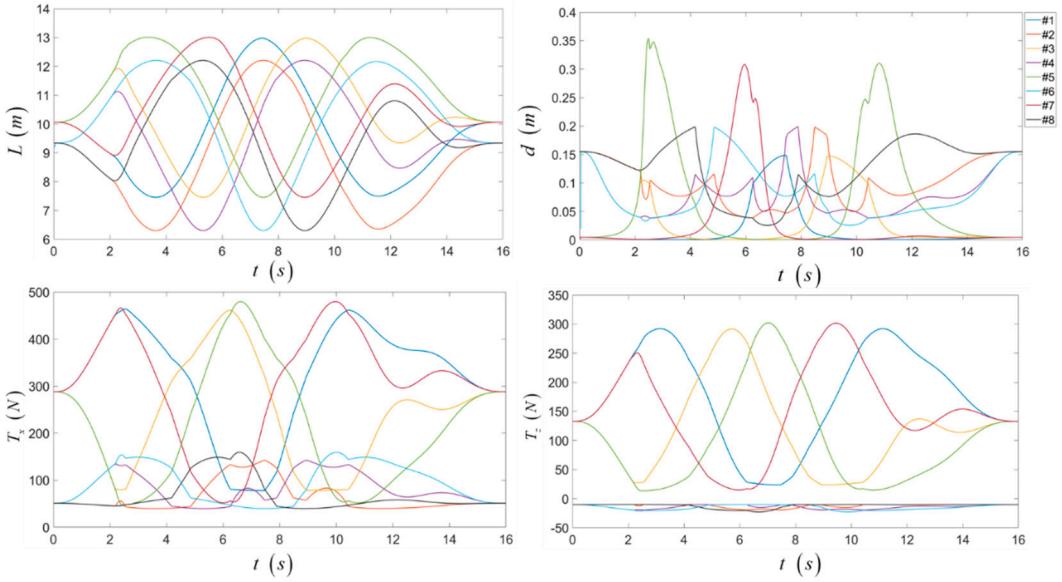

Figure 21. Unstrained length L, adjusting length d, tension along X-axis T_x and tension along Z-axis T_z respect to $\{A\}$ of CDPM that has the second configuration during the simulation test.

In the results of both configurations illustrated in Figures 20 and 21, our proposed model produces a continuous and smooth set of tension. In the second configuration, the T_x of cables remaining in bottom of the workspace is small in order to minimize the load of set of cables staying in the top, but still valid, since $T_x > -b_\pi/a_\pi$. This produces uneven load distribution and explains the good load capacity of the first configuration, as it has the same load but the highest load among cables of the second configuration, approximated as twice the first configuration. However, the solution is still applicable in both cases. In this test, we also make a simple controller that takes the tension forces as the input and responses by unstrained length L to simulate the motion of CDPMs. Thereby, the positioning accuracy of the moving platform is considered and illustrated in Figure 22.

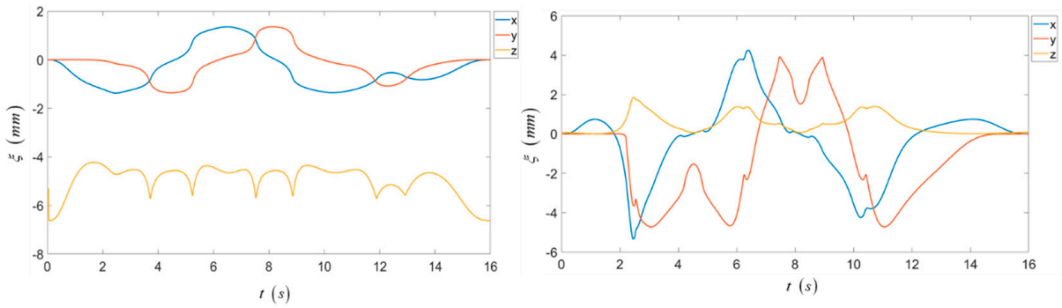

Figure 22. The positioning error of moving platform during the simulation test of both configuration (left: first configuration, right: second configuration).

The error of center of mass of moving platform during tracking on the desired trajectory is formulated in (56).

$$\xi(t) = \sum_i \mathbf{B}_i(t) - \mathbf{P}(t) \tag{56}$$

It can be seen that these errors are varying depending on the trajectory of moving platform and it does not tend to decrease over time. However, theoretically, our proposed model produces the new trajectory maintain positioning error around $(-6, 6)$ mm.

7.2. Experiment

Figure 23 illustrates our prebuilt spatial CDPM that contains two redundant actuators. Its configuration is similar to the first configuration of the simulated system and its main parameters are shown in Table 1. Figure 24 describes the control system of our prototype CDPM which consists of four similar groups. Each group contains two sets of actuator/sensors controlled by 1 PLC Siemens S7-1200. Each cable housed inside a winch is driven by a 220 V Delta AC Servo Motor ECMA-C20604RS with capacity of 400 W. The unstrained length and the cable tension force of cable is measured via an encoder and a load cell fixed on the winch, respectively. The value measured on the encoder will provide feedback to the driver, while the other, measured on the loadcell, is amplified and transmitted to PC via PLC. The PC is powered by Intel® core™ I3-2100 processor 3.10 MHz. It is used to generate and control signal for four groups through our application. One more response of PC is to synchronize signals from four PLCs, hence, the wireless communication is employed.

(a) **(b)**

Figure 23. Our prebuilt spatial CDPM with 2 redundant actuators used in experiment (**a**) perspective view; (**b**) end-effector.

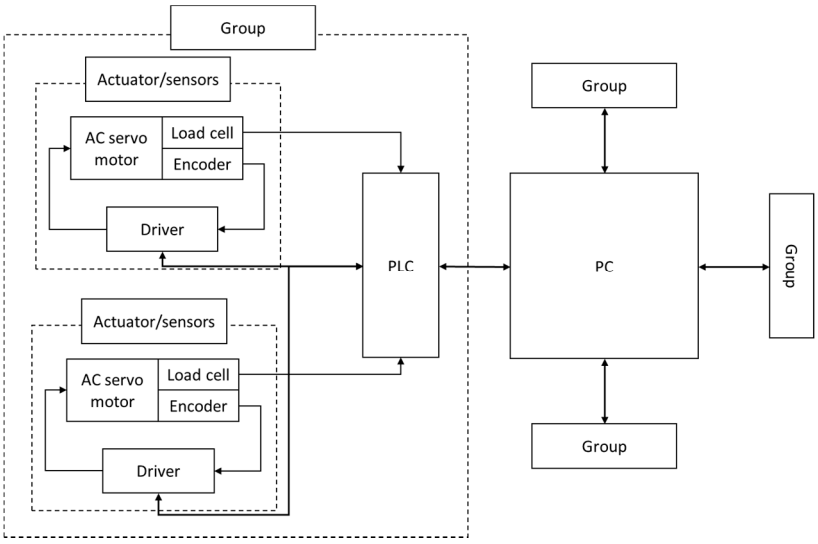

Figure 24. Diagram of the control system of our proposed prototype.

Due to the limit of technique in measurement positioning accuracy, the experimental evaluation is done in the static state. By employing the proposed method in static state, the valid minimum tension sets in the whole size of robot is obtained. The set of the testing position is randomly taken from this. Thereby, the proposed model is applied and the robot is controlled to these points. Our robot is ordered

to move point-to-point with the linear trajectory generated by the two-loop control system. The outer loop takes the cable tension forces and current pose of moving platform as its input, compares these values to the values of reference trajectory and aims at the response of the inner loop reference input. The inner loop is mainly based on the PID controller. It directly controls an actuator and feedback by the encoder. The linear trajectory is generated based on a 5th order trajectory generator with low speed. At each point, the robot is ordered to stop while measurement and error calculation is done.

Table 2 summarizes the test in this section, that includes testing desired positions, actual positions, and positioning errors obtained by applying Equation (56). Amplified load-cells and difference of cable lengths taken from encoders signals are also plotted in Figures 25 and 26 while the control system is manipulating the test. The test was done in about 14 min with 100 samples/s. However, for the convenience in tracking the signals while the moving platform is ordered to move to difference points, the intervals for stopping and calculating were replaced by vertical dash-lines represented in Figures 25 and 26. The test begins and finishes at home position $\mathbf{P}_0 = \begin{bmatrix} 0 & 0 & 1.5 \end{bmatrix}^T$. The torque fluctuation at the time the moving platform starts to move always has the largest amplitude and decreases gradually until it is stabilized, resulting in a jerk at the beginning. This is due to the overshooting of the PID controller. However, this jerk does not last long (about 2 s from the beginning) and the moving platform moves reliably for the rest of given trajectory.

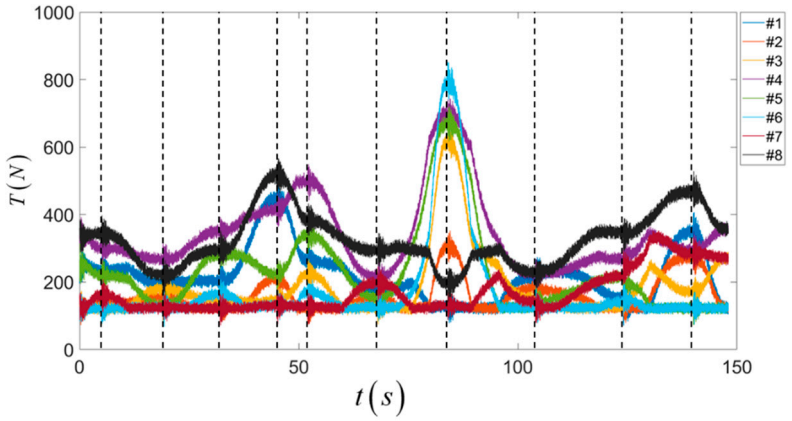

Figure 25. Amplified signals are taken from load-cells while the moving platform moves point-to-point with the linear trajectory.

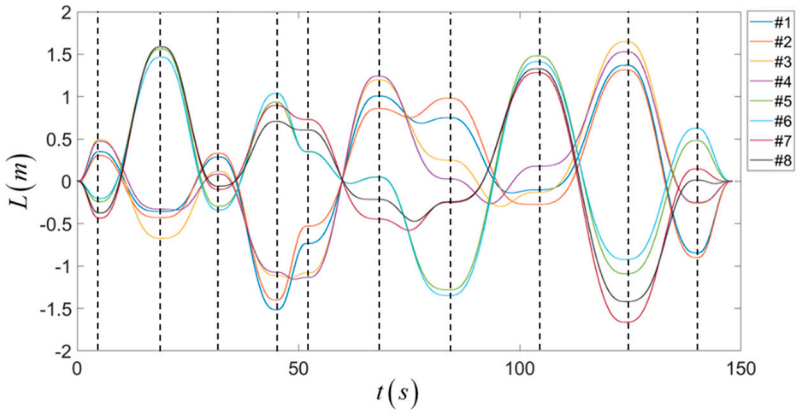

Figure 26. Different cable lengths are obtained by integrating the encoder signal while the moving platform moves point-to-point with the linear trajectory.

Figure 27 shows the position of the desired point of the moving platform in 3D. The size of each point indicates the positioning error. This error is produced by many sources: the accuracy of proposed model, the measurement method, the accuracy of measurers, non-ideal characteristics of cable material,

latency sync, transmission error and the cumulative error. According to the result of the experiment and our assumptions, the relationship between the desired position and positioning accuracy of the moving platform can be interpreted easily. Cable tensions at low altitude are smaller than those at high altitude. Furthermore, if the moving platform approaches a pole of robot fixed frame, then the force distribution is very unbalanced among cables. These reasons are also illustrated in Figure 25. On the other hand, the larger the cable tensions, the smaller the positioning error. In Figure 27, $\mathbf{P}_2$, $\mathbf{P}_8$ and $\mathbf{P}_6$ have a low altitude, resulting in the increase in positioning error. Meanwhile, points which have a high altitude (e.g., $\mathbf{P}_7$, $\mathbf{P}_5$ and $\mathbf{P}_4$), have a better accuracy.

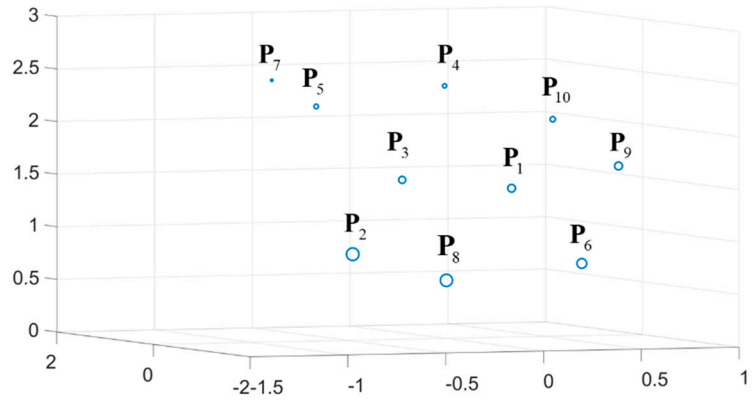

Figure 27. Set of static poses and the positioning error of the moving platform illustrated by the size of each point.

8. Conclusions

In this study, we introduced the model that use to solve the quasi-static problem of general spatial CDPM based on our simplified quasi-static model of a single cable. The explicit function that expresses the relationship between unstrained length L and tension exerted on free extremity **B** along the X-axis T_x is also concerned and applied to solve the inverse kinematic problem of CDPM. The main motivation of employing our model is that it is applicable in real-time and has a low mean positioning error. However, we cannot control the accuracy of the position of the moving platform due to an undefined feasible wrench workspace. Furthermore, the relation (48) is valid for as long as $T_x > T_{x_{\min}}$. Thus, for a better version, we propose some future work:

- Analyzing and determining the boundaries of the wrench-feasible workspace in order to determine the set of all wrenches that CDPMs can apply without violating the boundaries of the tensions and load capacities of actuators;
- Due to the presence of unstrained cables and large inertia of the moving platform, the vibration is easily identifiable in CDPM. Vibration has a great impact on the dynamic behavior of the positioning accuracy and deviation on force distribution. Therefore, having a good analysis of vibration is a premise to developing a good dynamic model.

Author Contributions: Conceptualization, N.T.T.; methodology, N.T.T.; software, P.G.L.; validation, P.G.L.; formal analysis, P.G.L.; resources, N.T.T.; data curation, P.G.L.; writing—original draft preparation, P.G.L.; writing—review and editing, P.G.L.; visualization, P.G.L.; supervision, N.T.T.; project administration, N.T.T.; funding acquisition, N.T.T. All authors have read and agreed to the published version of the manuscript.

Acknowledgments: This research was supported by Ho Chi Minh City University of Technology and Education, Vietnam.

Conflicts of Interest: The authors declare no conflict of interest

References

1. Vafaei, A.; Khosravi, M.A.; Taghirad, H.D. Modeling and control of cable driven parallel manipulators with elastic cables: Singular perturbation theory. In *International Conference on Intelligent Robotics and Applications*; Springer: Berlin/Heidelberg, Germany, 2011.
2. Alias, C.; Nikolaev, I.; Magallanes, E.G.C.; Noche, B. An Overview of Warehousing Applications based on Cable Robot Technology in Logistics. In Proceedings of the 2018 IEEE International Conference on Service Operations and Logistics, and Informatics (SOLI), Singapore, 31 July–2 August 2018.
3. Bosscher, P.; Williams, R.L., II; Bryson, L.S.; Castro-Lacouture, D. Cable-suspended robotic contour crafting system. *Autom. Constr.* **2007**, *17*, 45–55. [CrossRef]
4. El-Ghazaly, G.; Gouttefarde, M.; Creuze, V. Adaptive terminal sliding mode control of a redundantly-actuated cable-driven parallel manipulator: CoGiRo. In *Cable-Driven Parallel Robots*; Springer: Cham, Switzerland, 2015; pp. 179–200.
5. Oftadeh, R.; Aref, M.M.; Taghirad, H.D. Forward kinematic analysis of a planar cable driven redundant parallel manipulator using force sensors. In Proceedings of the 2010 IEEE/RSJ International Conference on Intelligent Robots and Systems, Taipei, Taiwan, 18–22 October 2010.
6. Lamaury, J.; Gouttefarde, M.; Chemori, A.; Hervé, P.-E. Dual-space adaptive control of redundantly actuated cable-driven parallel robots. In Proceedings of the 2013 IEEE/RSJ International Conference on Intelligent Robots and Systems, Tokyo, Japan, 3–7 November 2013.
7. Pott, A. An algorithm for real-time forward kinematics of cable-driven parallel robots. In *Advances in Robot Kinematics: Motion in Man and Machine*; Springer: Dordrecht, The Netherlands, 2010; pp. 529–538.
8. Pott, A.; Schmidt, V. On the forward kinematics of cable-driven parallel robots. In Proceedings of the 2015 IEEE/RSJ International Conference on Intelligent Robots and Systems (IROS), Hamburg, Germany, 28 September–2 October 2015.
9. Côté, A.F.; Cardou, P.; Gosselin, C. A tension distribution algorithm for cable-driven parallel robots operating beyond their wrench-feasible workspace. In Proceedings of the 2016 16th International Conference on Control, Automation and Systems (ICCAS), Gyeongju, Korea, 16–19 October 2016.
10. Gouttefarde, M.; Lamaury, J.; Reichert, C.; Bruckmann, T. A versatile tension distribution algorithm for $ n $-DOF parallel robots driven by $ n+ 2$ cables. *IEEE Trans. Robot.* **2015**, *31*, 1444–1457. [CrossRef]
11. Borgstrom, P.H.; Jordan, B.L.; Sukhatme, G.S.; Batalin, M.A.; Kaiser, W.J. Rapid computation of optimally safe tension distributions for parallel cable-driven robots. *IEEE Trans. Robot.* **2009**, *25*, 1271–1281. [CrossRef]
12. Yuan, H.; Courteille, E.; Deblaise, D. Elastodynamic analysis of cable-driven parallel manipulators considering dynamic stiffness of sagging cables. In Proceedings of the 2014 IEEE International Conference on Robotics and Automation (ICRA), Hong Kong, China, 31 May–7 June 2014.
13. Nguyen, D.Q.; Gouttefarde, M.; Company, O.; Pierrot, F. On the simplifications of cable model in static analysis of large-dimension cable-driven parallel robots. In Proceedings of the 2013 IEEE/RSJ International Conference on Intelligent Robots and Systems, Tokyo, Japan, 3–7 November 2013.
14. Riehl, N.; Gouttefarde, M.; Krut, S.; Baradat, C.; Pierrot, F. Effects of non-negligible cable mass on the static behavior of large workspace cable-driven parallel mechanisms. In Proceedings of the 2009 IEEE International Conference on Robotics and Automation, Kobe, Japan, 12–17 May 2009.
15. Merlet, J.-P.; Alexandre-dit-Sandretto, J. The forward kinematics of cable-driven parallel robots with sagging cables. In *Cable-Driven Parallel Robots*; Springer: Cham, Switzerland, 2015; pp. 3–15.
16. Kozak, K.; Zhou, Q.; Wang, J. Static analysis of cable-driven manipulators with non-negligible cable mass. *IEEE Trans. Robot.* **2006**, *22*, 425–433. [CrossRef]
17. Irvine, H.M. *Cable Structures*; The MIT Press: Cambridge, MA, USA, 1981; pp. 15–24.
18. Merlet, J.-P. Some properties of the Irvine cable model and their use for the kinematic analysis of cable-driven parallel robots. *Mech. Mach. Theory* **2019**, *135*, 271–280. [CrossRef]
19. Williams, R.L.; Gallina, P.; Rossi, A. Planar cable-direct-driven robots, part i: Kinematics and statics. In Proceedings of the 2001 ASME Design Technical Conference, 27th Design Automation Conference, Pittsburgh, PA, USA, 9–12 September 2001.
20. Gouttefarde, M.; Collard, J.-F.; Riehl, N.; Baradat, C. Simplified static analysis of large-dimension parallel cable-driven robots. In Proceedings of the 2012 IEEE International Conference on Robotics and Automation, Saint Paul, MN, USA, 14–18 May 2012.

21. Li, H.; Zhang, X.; Yao, R.; Sun, J.; Pan, G.; Zhu, W. Optimal force distribution based on slack rope model in the incompletely constrained cable-driven parallel mechanism of FAST telescope. In *Cable-Driven Parallel Robots*; Springer: Berlin/Heidelberg, Germany, 2013; pp. 87–102.
22. Gouttefarde, M.; Collard, J.-F.; Riehl, N.; Baradat, C. Geometry selection of a redundantly actuated cable-suspended parallel robot. *IEEE Trans. Robot.* **2015**, *31*, 501–510. [CrossRef]
23. Pott, A.; Mütherich, H.; Kraus, W.; Schmidt, V.; Miermeister, P.; Dietz, T.; Verl, A. IPAnema: A family of cable-driven parallel robots for industrial applications. In *Cable-Driven Parallel Robots*; Springer: Berlin/Heidelberg, Germany, 2013; pp. 119–134.